Characterization of combustion anomalies in a hydrogen-fueled 1.4 L commercial spark-ignition engine by means of in-cylinder pressure, block-engine vibration, and acoustic measurements

P.M. Diéguez[a], J.C. Urroz[a], D. Sáinz[a], J. Machin[a], M. Arana[a,b], L.M. Gandía[a,b,*]

[a] *School of Industrial & ICT Engineering, Public University of Navarre, Campus de Arrosadía, E-31006 Pamplona, Spain*

[b] *Institute for Advanced Materials (InaMat), Public University of Navarre, 31006 Pamplona, Spain*

[*] Corresponding author. Phone: +34 948 169 605. Fax: +34 948 169 606.

E-mail addresses: pmde@unavarra.es (P.M. Diéguez); lgandia@unavarra.es (L.M. Gandía).

Abstract

Abnormal combustion phenomena are among the main hurdles for the introduction of hydrogen in the transportation sector through the use of internal combustion engines (ICEs). For that reason the challenge is to guarantee operation free from combustion anomalies at conditions close to the ones giving the best engine output (maximum brake torque and power). To this end, an early and accurate detection of abnormal combustion events is decisive in order to allow the electronic control unit deciding suitable correcting actions. In this work, an automotive size 4-cylinder 1.4 L naturally aspirated port-fuel injection spark ignition Volkswagen engine adapted to run on hydrogen has been investigated. Three distinct methods (in-cylinder pressure, block-engine vibration and acoustic measurements) have been employed to detect abnormal combustion phenomena provoked through the enrichment of the hydrogen-air mixture fed to the cylinders under a wide range of engine speeds (1,000-5,000 rpm). It has been found that the high-frequency components of the in-cylinder pressure and block engine acceleration signals obtained after a Fourier transform analysis can be used for very sensitive detection of knocking combustion cycles. In the case of the ambient noise measurements, a spectral analysis in terms of third octave bands of the signal recorded by a microphone allowed an accurate characterization. Combustions anomalies could be detected through more intense octave bands at frequencies between 250 Hz and 4 kHz in the case of backfire and between 8 kHz and 20 kHz for knock. Computational fluid dynamics simulations performed indicated that some characteristics of the engine used such as the cylinder valves dimensions and the hydrogen flow rate delivered by the injectors play important roles conditioning the likelihood of suffering backfire events.

Keywords: Backfire; Hydrogen; Internal combustion engine; Knock; Noise; Pre-ignition.

Nomenclature

ABDC	after bottom dead centre
ATDC	after top dead centre
BDC	bottom dead centre
BTDC	before top dead centre
CA	crank angle (º)
CFD	Computational Fluid Dynamics
CR	compression ratio
DI	direct injection
EVC	exhaust valve closing

H_2-ICE	hydrogen-fueled ICE
ICE	internal combustion engine
MAP	manifold air pressure
MBP	maximum brake power (kW)
MBT	maximum brake torque (N·m)
n	engine speed (rpm)
NO_x	nitrogen oxides (ppm)
PCC	Pearson's correlation coefficient
PFI	port-fuel injection
RON	Research Octane Number
SA	spark advance (° BTDC)
SI	spark ignition
t	simulation time: time passed from the piston positioning at TDC (s)
t_0	time passed between the intake valve opening and the piston reaching TDC (s)
TDC	top dead centre
WOT	wide open throttle
Z_{iv}	intake valve positioning (m)
Z_p	piston positioning (m)

Greek letters

λ	air-to-fuel ratio
$\omega_{H_2}^{im}$	fraction of hydrogen injected in the intake manifold after intake valve closing, %

1. Introduction

Hydrogen of renewable origin has potential to play a relevant role in a more sustainable and environmental-friendly future transportation sector [1,2]. Whereas big R&D efforts are being directed toward vehicles mounting electric engines fueled by fuel cells or batteries, less attention is being paid to the internal combustion engines (ICEs) fueled with hydrogen or mixtures of hydrogen with other fuels such as methane (natural gas or biogas) [3,4]. In spite of their intrinsically low thermodynamic efficiency, ICEs fueled with hydrogen (H_2-ICEs) have the appealing advantages of being very robust and of requiring relatively easy and cheap modifications of the conventional gasoline-fueled ICEs running on hydrogen [5-9]. H_2-ICEs would speed up, at least as a transitory technology, the incorporation of hydrogen into the transportation sector.

Even though hydrogen exhibits some properties making it a very convenient fuel for use in ICEs such as wide range of flammability limits in air (4-75 vol. % H_2) that facilitate both fuel-lean (in practice air-to-fuel ratios $\lambda < 4$) and fuel-rich operation, and very rapid combustion rates that improve the process efficiency (*i.e.* the indicated fuel conversion efficiency that can be determined from a thermodynamic analysis of the engine operating cycle [10]), other characteristics have less desirable effects [11,12]. In this regard, the low density of H_2, the increased NO_x emissions due to the high flame temperatures, and its propensity for producing abnormal combustion phenomena are key factors that limit the power output of H_2-ICEs. The limitations introduced by the low density of H_2 can be offset using suitable combustion mixture formation strategies such as supercharging and unthrottled operation at variable λ for spark-ignition (SI) port-fuel injection (PFI), SI direct-injection (DI) of H_2 in the cylinders, or even compression ignition DI. However, the strong influence of the combustion mixture composition on the engine power output, NO_x emissions and combustion anomalies makes very challenging selecting the best H_2-ICE operating conditions [13,14]. Verhelst and Wallner have analyzed the possible control strategies that can be adopted for optimizing the trade-off existing between engine power output on the one hand, and NO_x emissions and combustion anomalies on the other, that hinders operating H_2-ICEs at or near stoichiometric fuel-air mixtures [15].

As concerns the abnormal combustion phenomena, they are, of course, not unique to H_2-ICEs as they are typical problems for the improvement of the thermal efficiency of conventional engines running on liquid fuels [10,16-17]. Combustion anomalies can be classified into three main categories: pre-ignition, backfire and knock [15], although the actual situation is much more complex due to the interaction between these phenomena [10]. For example, the occurrence of pre-ignition increases the likelihood of suffering backfire or knock in the next combustion cycles [18]. In any case, all of them consist in unscheduled combustion events that have negative effects on the engine performance. These effects can vary from a big loss of power output in the case of pre-ignition to the risk of severe damage of engine components in the case of backfire and knock. They can be distinguished by their origin and timing within the engine operating cycle. Pre-ignition and backfire are caused by hot spots inside the combustion chamber (spark plug electrodes, hot valves, oil ash, etc. [12]) that ignite the fuel-air mixture before the spark plug fires in SI engines. Pre-ignition takes place typically during the early stages of the compression stroke whereas backfire, also known as backflash, occurs during the intake stroke of engines with external fuel-air mixture formation systems. As the intake valves are still open, mixture combustion can extend to the intake manifold resulting that, in addition to the loss of torque output, backfire can cause strong damage of the mixture formation and fuel injection systems. The wide range of flammable H_2-air mixture compositions and the low energy required to ignite these mixtures that, as a matter of fact, reaches a minimum for the stoichiometric composition [12,15], are the main reasons for the tendency of H_2 to suffer from pre-ignition. Backfire problems can be reduced adopting fuel DI strategies; moreover, minimizing the possible causes of hot spots formation will obviously help to operate an engine reasonably free from pre-ignition and backfire. To this end, suitable design and maintenance of the fuel injection and engine cooling systems are very important. The fact that H_2 combustion does not generate particulates is an advantage in this regard.

In contrast to pre-ignition and backfire, knock occurs in SI engines after the spark plug has fired and a flame front has been formed inside the cylinder. It takes place within the so-called knock window that goes from the late stages of the compression stroke when the piston is very near to the top dead centre (TDC) to several crank angle (CA) degrees at the beginning of the expansion stroke [19]. End-gas conditions change rapidly with flame propagation. Particularly, the temperature and pressure increase markedly as a result of the heat generated by the flame front and the compression due to the motion of the piston and the expansion of the hot combustion products thus leading to an acceleration of the combustion reactions rate. If the conditions are such that the concentration of free radical chemical species reaches critical values [18], spontaneous auto-ignition of the unburned gases can take place without the participation of any ignition source. This occurs at one or more points inside the end-gas region (typically near the cylinder walls [10,20]) giving rise to knock. This phenomenon has stochastic nature and the increase of pressure produced can reach peak values of several thousands of kPa in the case of heavy knock. Moreover, high-frequency oscillating pressure waves are generated that consist in acoustic vibration modes characteristic of the combustion chamber geometry. These waves are transmitted through the metallic structure causing engine vibration and a very characteristic sharp metallic (pinging) noise. In the event of prolonged heavy knock, the strong thermal and mechanical stresses suffered by the components of the combustion chamber may result in severe engine damage (piston ring sticking or breakage, cylinder head gasket failure, cylinder head erosion, piston melting, etc. [10]). Obviously the severity of knock will be higher at high engine loads and under any operating circumstance allowing the mass of auto-ignited end-gas to be a large fraction of the fresh charge. For that reason the spark advance (SA) becomes a key operating parameter to be optimized for obtaining the maximum brake torque (MBT) possible under knock-free conditions [21]. Exhaust gas recirculation has been also identified as an effective strategy to suppress knock [22].

Knock also depends greatly on the fuel properties and combustion chemistry [23]. In this regard, the induction time is defined as the time needed for some critical chemical species to reach a given concentration that allows initiating the combustion chain reactions by auto-ignition [10]. It is widely accepted that when the end-gas temperature and pressure are such that the induction time becomes lower than the time required to combust the whole fresh charge by flame propagation the knock phenomenon will likely take place [24]. On the other hand, the end-gas heterogeneities are key in determining the auto-ignition mode [18].

There is some controversy in the literature regarding the tendency of H_2 to originate knock. The very high auto-ignition temperature and combustion rate of H_2 are factors that should contribute to an increased resistance to knock compared to the conventional liquid fuels. However, wide variations in flame propagation rates taking place during combustion when operating on pure H_2 have been considered to increase the risk of suffering from combustion anomalies [23]. The debate is due in part to the very different octane numbers reported for H_2 that in the case of the Research Octane Number (RON) range from 60 [25] to above 120 [12]. Verhelst and Wallner have discussed on these discrepancies pointing out that they are due to the experimental difficulties introduced by the high rate of H_2 combustion in air under stoichiometric conditions and the strong dependence of the reaction rate on mixture composition [15]. As pointed out by these authors, it is questionable using octane ratings to measure the knock resistance of H_2 because these standardized methods were developed for liquid fuels. Tang *et al.* [26] did not detect knock during an investigation carried out with an automotive-size 2.0 L PFI H_2-ICE. It should be noted that this study was carried out with the engine running unthrottled on lean mixtures with λ values between 1.4 and 3. The only abnormal phenomenon noticed was pre-ignition that was observed when the engine was run on the richest H_2-air mixture considered (λ = 1.4) at compression ratio (CR) of 14.5:1 and engine speed of 3,000 rpm. However, several studies dedicated to investigate the onset mechanism, detection and characterization of knock reveal that this phenomenon is an important problem for H_2-ICEs fueled with stoichiometric or near-stoichiometric H_2-air mixtures [23,25-33]. As a result, key parameters such as CR, λ, and SA should be carefully selected in order to be able of giving the highest possible torque output at any time without knocking. Unfortunately these limitations give rise to a remarkable decrease of the peak power output compared to that of the operation with gasoline. In this regard, peak power values up to 35 % lower at low and moderate engine speeds and up to 50 % lower at the highest speeds (6,000 rpm) have been reported [5].

Most studies on knock occurrence in H_2-ICEs have been performed using single-cylinder research engines at moderate or low speeds [23,27-30]. On the other hand, investigations carried out on automotive-sized H_2-ICEs did not observe knock [26,33] or focused on recording the in-cylinder pressure trace for detecting knock [25] or studying the distinctive characteristics of knock produced by H_2 auto-ignition [31,32]. In this context, a commercial SI Volkswagen engine adapted to run on hydrogen (PFI) has been employed in this work to investigate H_2 combustion anomalies. Three techniques based on the in-cylinder pressure, block engine vibration and ambient acoustic measurements have been employed. The data obtained have been analyzed to detect and characterize abnormal combustion events under a wide range of engine speeds. To our knowledge, there is no previous study similar to this one performed on automotive-size H_2-ICEs, especially as concerns noise measurements. Finally, computational fluid dynamics (CFD) simulations have been performed in order to assess to what extent the characteristics of the adapted commercial engine used can influence on some of the abnormal combustion phenomena detected, particularly backfire.

2. Engine characteristics, experimental setup and methods

The engine and test facility used in this study were described in detail elsewhere [4,6]. Briefly, a Volkswagen 4-cylinder 1.4 L naturally aspirated PFI SI engine with a CR of 10.5:1 was employed. It gave maximum brake power (MBP) and MBT of 59 kW at 5,000 rpm and 132 N·m at 3,800 rpm, respectively, when fueled with gasoline. The engine was adapted to run on H_2 resulting in a significant performance reduction (MBP of 32 kW at 5,000 rpm and MBT of 63 N·m at 3,800 rpm) due in great part to the conservative operating conditions employed. As concerns the test bed cell, it consisted of an eddy current dynamometer AVL 80 [4,6]. Hydrogen and air flow rates were determined using mass-flow meters (Bronkhorst) with a precision of ± 0.5 %. Pressure and temperature in the intake manifold were recorded with a Bosch 03C.906.051 apparatus. The CA and pressure in cylinder number 1 were measured with Kistler 2613B1 (± 0.02 º) and 6117B (± 0.6 %) sensors, respectively. The exhaust gases were analyzed with a Horiba MEXA-720NOx analyzer for NO_x determination with an accuracy of ± 30 ppm.

As for the block engine vibrations produced by abnormal combustion events they were measured using an accelerometer [34-36]. As a matter of fact this type of sensors are typically mounted on the commercial automotive engines fabricated in series. Whereas in-cylinder pressure measurements are typical at the laboratory scale, this technique is too costly to be implemented in commercial vehicles [27]. In this work, a Bruel & Kjaer 4504 tri-axial piezoelectric CCLD accelerometer (range: 1-10,000 Hz; sensitivity: 10 ± 20 % mV/g) was used and placed near the head of the cylinder in which the combustion anomalies were recorded. Preliminary experiments showed an excellent agreement between the responses of the original accelerometer and the one mounted on the engine-block. The most intense signals were obtained in the direction parallel to the axis of the cylinders. Only the data recorded in that direction will be presented.

One of the main novelties of this work is that ambient sound measurements have been also performed to characterize abnormal combustion events. The acoustic measurements were conducted in the engine test bed cell that behaved as an almost semi-anechoic room. Sound pressure was recorded using a G.R.A.S. 40AC high-precision condenser microphone (up to 40 kHz with a sensitivity of 12.5 mV/Pa) placed 1 m from the engine.

After starting up the engine using an initial λ of 1.7, it was let idle for a few minutes for suitable warming. The experiments were performed in such a way that the H_2-air mixture fed to cylinder number 1 was enriched in the fuel (decreasing values of λ) by increasing the H_2 injection pulse width stepwise until that combustion anomalies appeared. In most of the experiments, only one cylinder was fed with the enriched mixture in order to prevent the engine from suffering severe damage. The process was repeated at engine speeds ranging from 1,000 rpm to 5,000 rpm and full load (wide open throttle, WOT). SA was set at 10 º BTDC whereas the exhaust valves closed at CA of 3 º after top dead centre (ATDC) and the H_2 injection started at CA of 22 º ATDC during the intake stroke. SA value was selected according to our previous experience with the engine that showed that 10 º BTDC constitutes a trade-off between satisfactory engine performance and combustion anomalies [4,6,8]. Abnormal combustion occurrence could be detected by a characteristic pinging noise followed by a strong bass noise accompanied by a great decrease of the brake torque. Once that point was reached the engine was shut off.

To guarantee a correct characterization free from unwanted signals, data used for abnormal combustion events detection (in-cylinder pressure, accelerometer and microphone signals) were recorded with a sufficiently high frequency of 100 kHz. On the other hand, the parameters related with the engine operation (engine speed, λ, intake manifold temperature and pressure, injection pulse width and NO_x concentration in the exhaust gases) were registered with a frequency of 10 Hz. Another important aspect is the number of engine cycles analyzed. Brunt *et al.* recommended a sample of at least 1,000 cycles for a suitable determination of the intensity of the combustion events on a Ford Zetec 2.0 L 4-cylinder engine fueled with gasoline [37]. In our case the samples ranged from 1,224 cycles at engine speed of 1,000 rpm to 3,275 at 3,000 rpm and 2,725 cycles at engine speed of 5,000 rpm. This resulted in experiments lengths ranging from 147.2 s at 1,000 rpm to 65.6 s at 5,000 rpm.

3. Results and discussion

3.1. Abnormal combustion characterization

In contrast to block-engine vibration and sound measurements, the in-cylinder pressure values give a direct measure of the dynamics of the combustion process. Fig. 1 shows an example comparing the characteristics of normal and abnormal combustion cycles recorded at the highest engine speed (5,000 rpm) and λ = 1.52. The graph shows the evolution with CA of the pressure (gauge) in cylinder number 1. Note that the origin of the CA axis is situated at spark time (350 º= 10 º BTDC). Data along a CA period of 50 º characterized by the highest in-cylinder pressures are provided. This CA window is slightly higher than the range of 40 º from TDC recommended by Brunt *et al.* in a study performed with an automotive-sized engine [37]. As can be seen, during the normal combustion cycle the in-cylinder pressure increases gradually after the spark plug fires until reaching a maximum value of about 53 bar at TDC. The cycle showing knock is characterized by high-frequency pressure oscillations with a maximum amplitude of about 20 bar leading to a peak pressure close to 84 bar also at TDC. This almost doubles the pressure rise rate of 1.0 MPa/CA considered as the lower limit for heavy knock [24]. The amplitude of the pressure oscillations decreases progressively ATDC although the oscillations are still present at CA of 40 º ATDC during the expansion stroke. It can be observed that during the knocking cycle the in-cylinder pressure rises more rapidly than during the normal combustion cycle in accordance with Li and Karim [23]. Presumably this lowers the induction or delay time leading to the occurrence of a spontaneous auto-ignition of the end-gas [24]. Cycle-to-cycle combustion variations and flame instabilities may also result in a temperature increase and thermal inhomogeneity that facilitate reaching the critical conditions that provoke knock [24,32]. According to Li *et al.* [38] the energy density and heat release rate in hot spots play critical roles in determining knock intensity. In the case of backfire the in-cylinder pressure is very low and shows a very smooth decrease during the expansion stroke. This is due to the fact that the fuel has been already burned during the previous intake stroke.

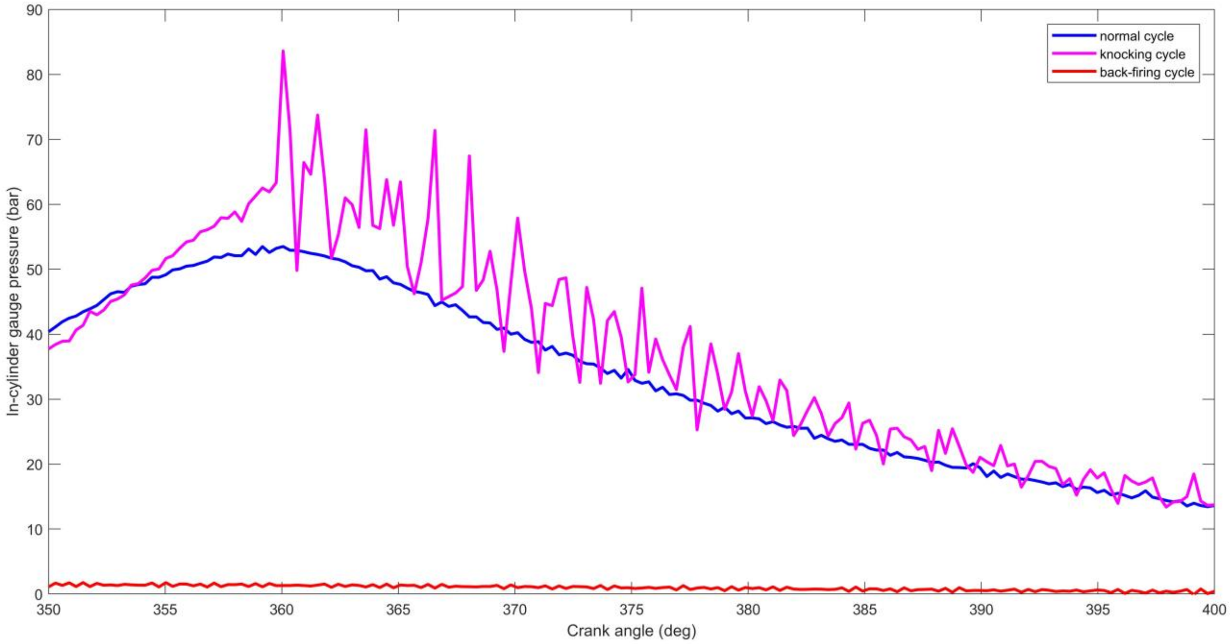

Fig. 1. Evolution of the in-cylinder pressure with CA at engine speed of 5,000 rpm for the following cycles: normal cycle, knocking cycle, and backfiring cycle.

A more complete characterization of the abnormal combustion phenomena is given in what follows taking as base case the experiments performed at an intermediate engine speed of 2,000 rpm. Fig. 2 shows the evolution along time of the in-cylinder pressure, accelerometer and microphone signals and the temperature in the intake manifold. On the other hand, Fig. 3 depicts the evolution of the parameters characterizing the engine performance for the same experiments. The width of the hydrogen injection pulse was increased from its initial value of 6.2 ms (λ = 1.7) resulting in a progressive decrease of the λ value. After 100 s the pulse width was about 6.9 ms (λ = 1.45) and the brake torque reached an almost steady value of 57 N·m. The NO_x concentration and in-cylinder pressure also increased reaching 430 ppm and 60 bar, respectively. On the other hand, the accelerometer and microphone recorded normal signals of ± 15 g and ± 5 Pa, respectively.

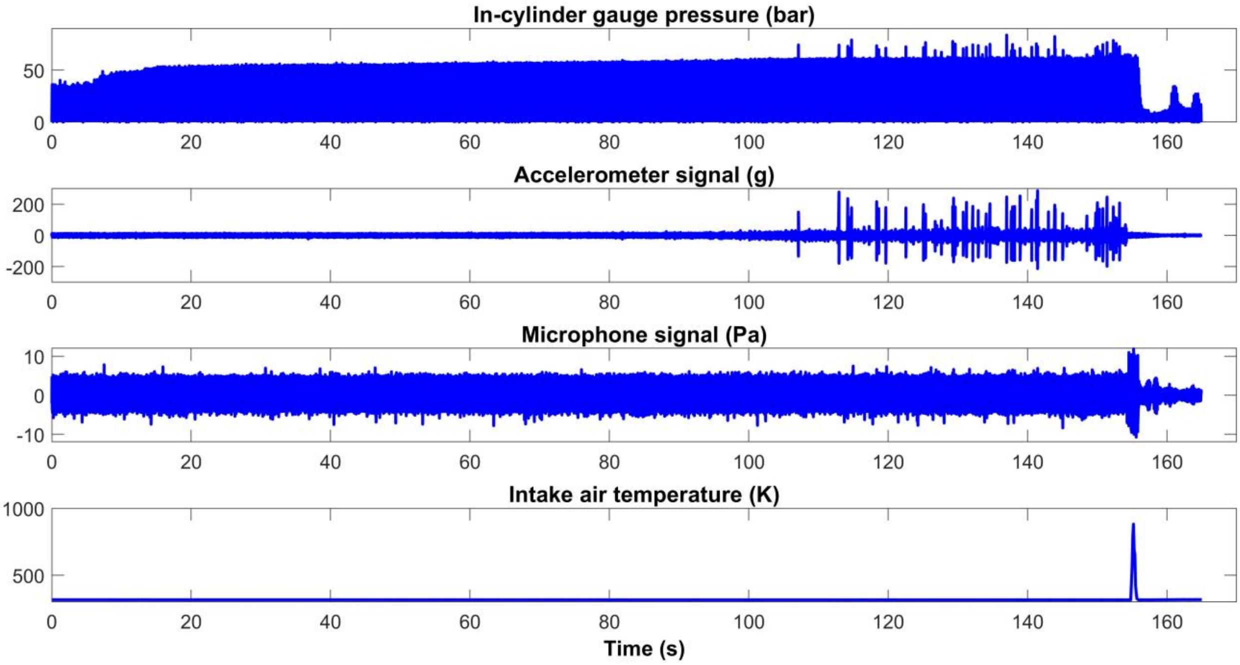

Fig. 2. Evolution with time of the parameters used for the characterization of abnormal combustion phenomena at engine speed of 2,000 rpm. From top to bottom: in-cylinder pressure, accelerometer signal, microphone signal, and intake air temperature.

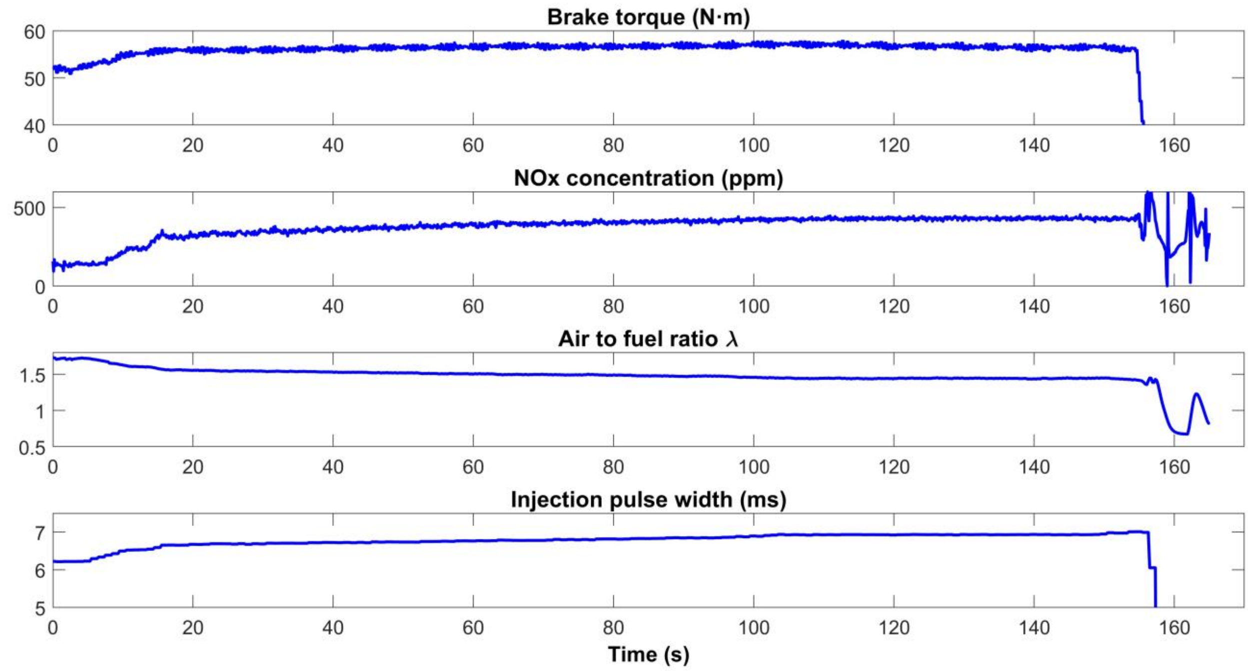

Fig. 3. Evolution with time of the performance parameters at engine speed of 2,000 rpm. From top to bottom: brake torque, NO_x concentration in the exhaust gases, air-to-fuel ratio (λ) and H_2 injection pulse width.

As can be seen in Fig. 2, the first knock event was registered after 107 s, when strong signals of ± 160 g and 75 bar, were recorded by the accelerometer and the pressure sensor, respectively. This event was audible and it was decided to maintain constant the hydrogen injection pulse width; however, the microphone did not register any clear signal distinguishable from the background noise. At this point the engine entered a 40 s period characterized by strong vibrations reaching an amplitude of up to + 300 g, and pressure peaks of up to above 80 bar; a characteristic pinging noise could also be heard. During this period the brake torque showed a very slight tendency to decrease whereas the NO_x emissions remained essentially unchanged (see Fig. 3). After 155 s a strong hoarse noise was produced that could be recorded by the microphone (amplitude of up to + 10 Pa). This was followed by an abrupt decrease of the in-cylinder pressure and the brake torque and erratic readings of the exhaust NO_x concentration. This last event consisted in backfire as deduced from the intense increase of the intake air temperature produced. At that moment the engine was switched off.

Similar results (not shown) were observed at 1,000 rpm, 4,000 rpm and 5,000 rpm, whereas at 3,000 rpm no knock was detected by the sensors and the engine passed directly from normal running to backfire. However, by increasing the spark advance from 10 º BTDC to 20 º and 30 º BTDC knock was detected before backfire also at 3,000 rpm. It should be noted that if ignition is started far from TDC there is a higher likelihood of suffering knock and of producing more intense pressure oscillations [23]. Moreover, spark advance becomes critical in the case of engine operation under lean-burn conditions due to more pronounced cycle-to-cycle combustion variations that also contribute to increase knock likelihood [39].

3.2. Knocking combustion cycles: analysis of the in-cylinder pressure and accelerometer signals

As shown in the previous section, knock could be identified by means of the abrupt variations of the readings recorded by the in-cylinder pressure transducer and the block engine accelerometer. Now the correlation between these two signals is analyzed.

Mass-elastic systems show natural vibration frequencies so that for a given frequency the system vibrates according to characteristic amplitude and phase which is known as a vibration mode. Only some of the lowest order frequencies are of practical interest because the high-order ones are generally significantly damped. In the case of ICEs, combustion (both normal and abnormal) and motion of engine components cause vibrations that are transmitted through the engine structure. Of course, the intense in-cylinder pressure oscillations associated to knock provoke stronger vibrations that can be detected with an accelerometer. This is the reason why commercial engines mount these simple sensors for knock detection and engine operation control and management instead of the much more expensive and complex in-cylinder pressure transducers and optical sensors [35,36].

In this work, distinction between high and low frequencies has been made taking as reference the values above and below 20 times the engine speed, respectively. According to this criterion, Fig. 4 and Fig. 5 show typical readings of the in-cylinder pressure transducer and the accelerometer, respectively, for normal and knocking combustion cycles. Signals were decomposed into their low- and high-frequency components by means of Fourier transform (FT) analysis. In both cases the engine speed was 2,000 rpm and the signals corresponded to the values recorded within spark time (10 º BTDC) and 40 º ATDC. It can be seen that for the normal combustion cycles the pressure signal coincides with the low-frequency component whereas the accelerometer signal is very weak and indistinguishable from the low- and high-frequency components. In the case of the knocking cycles, the pressure signal is dominated by the low-frequency component whereas the oscillations are well represented by the high-frequency component. In contrast, the accelerometer signal is dominated by the high-frequency component as can be seen in Fig. 5.

It can be then concluded that the high-frequency component of the in-cylinder pressure and block engine acceleration signals obtained after a FT analysis can be used for very sensitive detection of knock events in H_2-ICEs of automotive size. Making the distinction between low and high frequency on the basis of the engine speed is useful to take into account at every moment the influence of this key parameter on the engine vibration characteristics because other factors such as the engine geometry, the speed of sound, etc. will not change significantly. A value of 20 times the engine speed was adopted after a preliminary screening. The exact value of this reference is not very critical provided it is relatively close to the engine speed which seems reasonable.

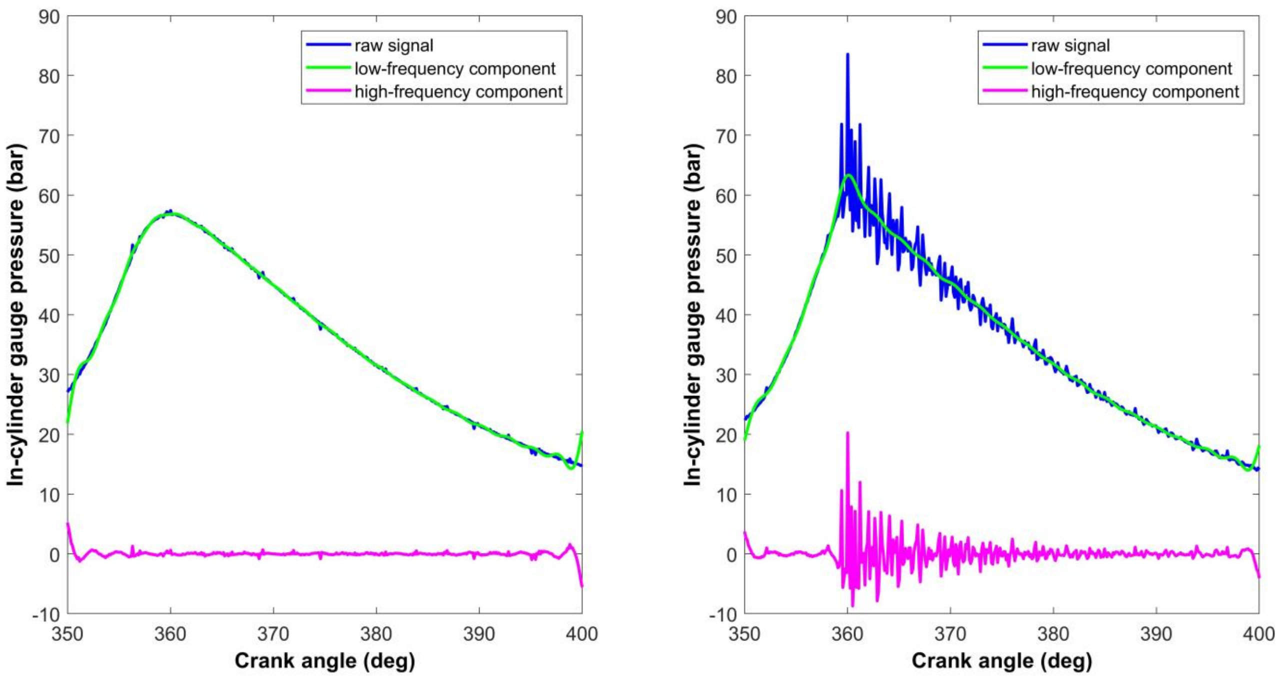

Fig. 4. Evolution of the in-cylinder pressure with CA at engine speed of 2,000 rpm for typical normal (left) and knocking (right) combustion cycles showing the in-cylinder transducer raw signal and its low-frequency and high-frequency components.

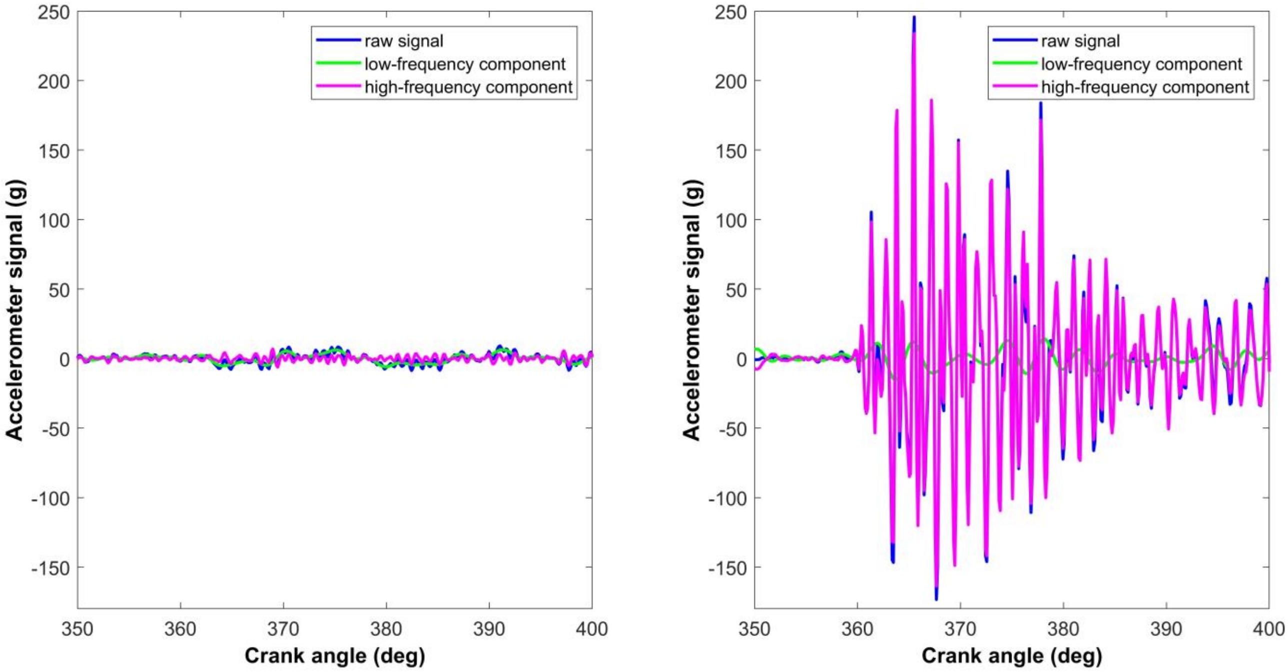

Fig. 5. Evolution of the acceleration with CA at engine speed of 2,000 rpm for typical normal (left) and knocking (right) combustion cycles showing the accelerometer raw signal and its low-frequency and high-frequency components.

A further analysis of the sensors signals has been performed through the study of the evolution of the integral average of the high-frequency components' modulus. This is shown in Fig. 6 and Fig.7 for the readings from the accelerometer mounted on the block engine and the in-cylinder pressure transducer, respectively. For each engine speed considered, the possible linear correlation between the accelerometer and the pressure transducer signals has been assessed through the values of the Pearson's correlation coefficient (PCC). In these experiments, the air-to-fuel ratio (λ) of the mixture decreases from cycle to cycle due to a gradual increase of the H_2 injection pulse width. The high values of the integral averages observed after about 2,000 cycles indicated the appearance of knock events. When the complete datasets are considered, the PCC values obtained at 2,000 rpm, 4,000 rpm and 5,000 rpm are 0.701, 0.613 and 0.699, respectively, that, given the large size of the samples, indicate a high degree of linear correlation. It should be noted that no knocking cycles were detected at 3,000 rpm so data corresponding to that engine speed were not considered. In contrast, the PCC at engine speed of 1,000 rpm was only 0.200 thus revealing lack of linear correlation between the signals. This is a low speed regime for an automotive size engine, close to idling. This is a fluctuating regime showing speed oscillations around the set point that provoke in-cylinder pressure instabilities. This can be appreciated in Fig. 7 where at 1,000 rpm the in-cylinder pressure changes gradually during the first combustion cycles until the reading is stabilized. These relatively smooth pressure changes do not translate to the acceleration signal due to its inertial character that results in remarkable damping. If the cycles preceding the 220 one at 1,000 rpm are discarded the PCC increases from 0.200 to 0.819 showing strong liner correlation also at this speed.

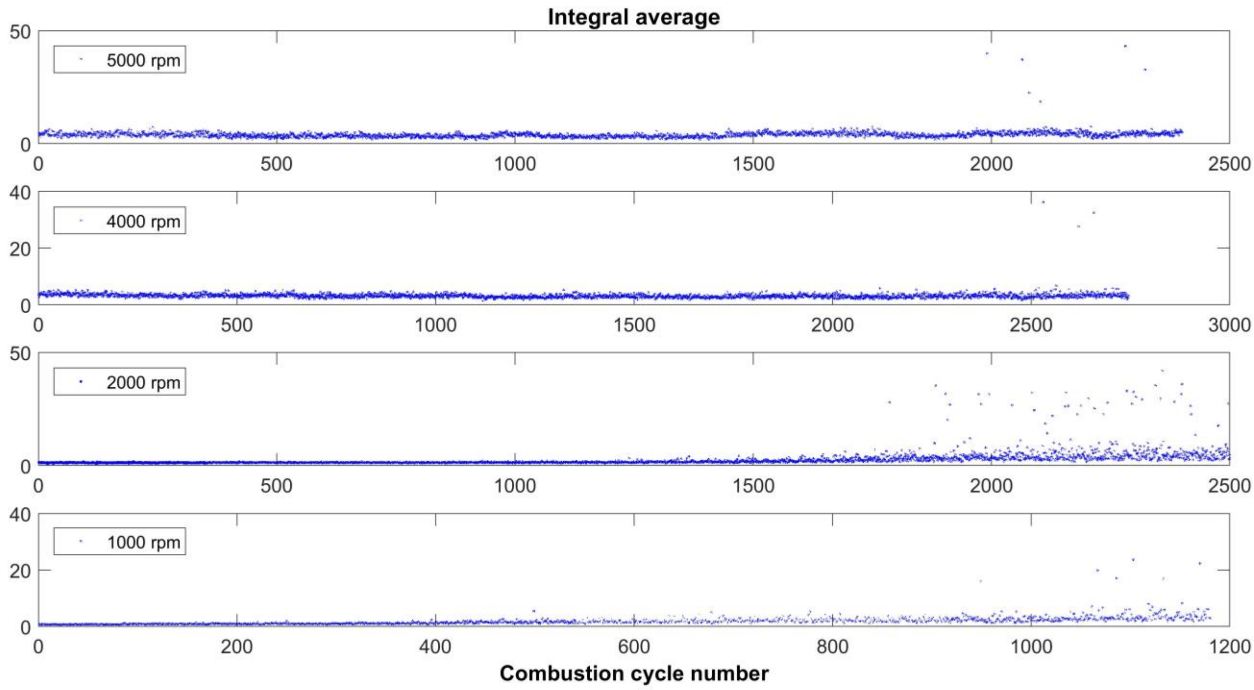

Fig. 6. Evolution of the integral average of the high-frequency components' modulus of the accelerometer signal for each of the combustion cycles indicated at engine speeds of (from bottom to top): 1,000 rpm, 2,000 rpm, 4,000 rpm and 5,000 rpm.

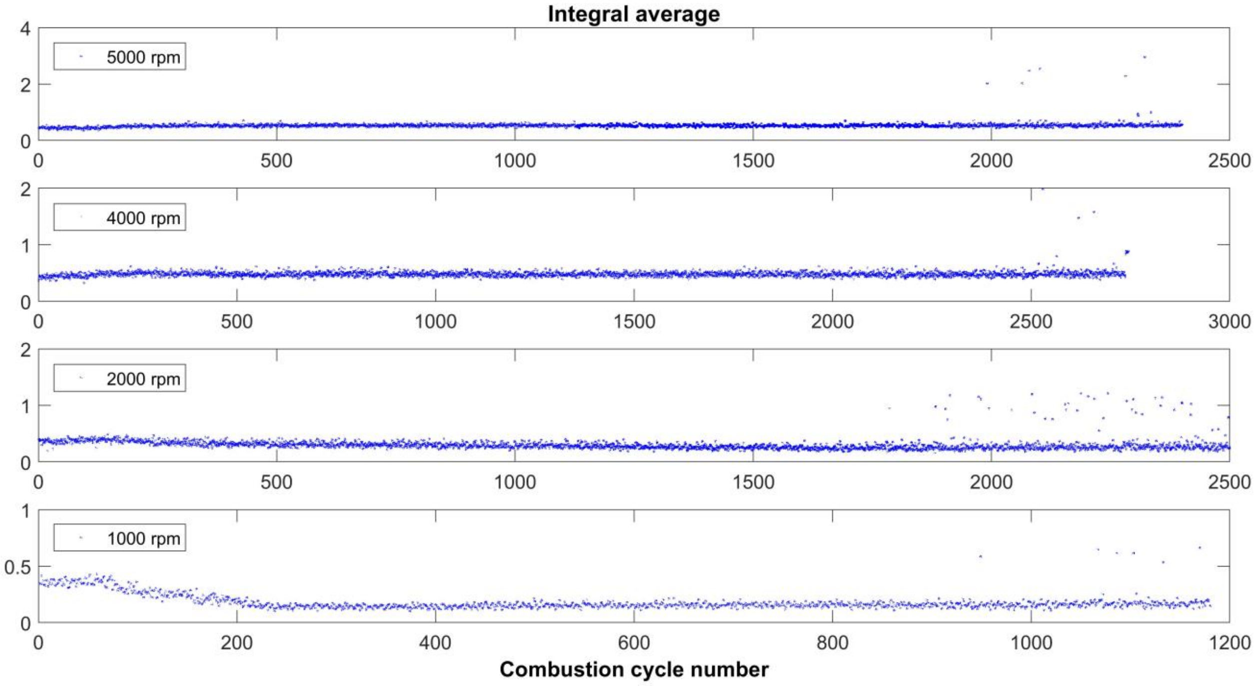

Fig. 7. Evolution of the integral average of the high-frequency components' modulus of the in-cylinder pressure signal for each of the combustion cycles indicated at engine speeds of (from bottom to top): 1,000 rpm, 2,000 rpm, 4,000 rpm and 5,000 rpm.

A more detailed observation of Fig. 7 suggests that knocking combustion cycles are characterized by values of the integral average of the high-frequency components' modulus of the in-cylinder pressure signal above 0.5. From the 2,500 combustion cycles shown in Fig. 7 at engine speed of 2,000 rpm only 39 cycles fulfill this criterion. The PCC for the high-frequency components of the accelerometer and the pressure transducer signals during these cycles is 0.584 thus indicating a practically linear correlation. On the other hand, at engine speed of 5,000 rpm only 9 cycles seemed to present knocking events but in this case the PCC was - 0.294 which indicates that the correlation between the signals losses relevance at high engine speeds. The reason could be the inertial nature of the vibrations leading to the signal captured by the accelerometer. Knock generates vibrations that require time to be completely damped, especially the low-frequency vibration modes. Therefore, normal combustion cycles can be mistakenly identified as knocking ones if one or several of the preceding cycles suffered from abnormal combustion events. As the engine speed increases this possibility is more likely because the time interval available for vibrations damping among consecutive combustion cycles decreases. In this regard, if the correlation investigated is among the integral average values of the high-frequency components' modulus of the in-cylinder pressure signal of the 9 knocking cycles and those of the accelerometer signal for the cycles just following the knocking ones [27], the PCC reaches a much higher value of 0.537. The silentblocks incorporated into the commercial engines for absorbing vibrations and reducing noise introduce non-linearity among the in-cylinder pressure and engine block acceleration thus complicating the rapid identification of knock. As a result, the criteria used to identify knock with accelerometers mounted on the block engine should be more restrictive and be adapted to the engine speed. From the results shown in Fig. 6 it can be suggested that whereas integral average values of the high-frequency components' modulus of the accelerometer signal above 15 can be used at engine speeds below 2,000 rpm, this limit has to be increased to about 30 for higher speeds.

3.3. Engine noise analysis

As already mentioned, one of the main novelties of this work is the use of ambient noise measurements to identify abnormal combustion events. It is well known that phenomena such as knock is accompanied by a characteristic pinging noise so it is interesting to explore the possibility of using acoustic measurements for the detection of abnormal combustion. Fuel combustion produces the so-called combustion noise, which is the most important source of noise in an ICE. Combustion noise is a complex phenomenon affected by the characteristics of the fuel as well as that of the engine and its operating conditions [40].

Returning to the results shown in Fig. 2 and corresponding to an engine speed of 2,000 rpm, Fig. 8 and Fig. 9 show the instantaneous values of the in-cylinder and acoustic pressures for a series of normal and knocking combustion cycles, respectively.

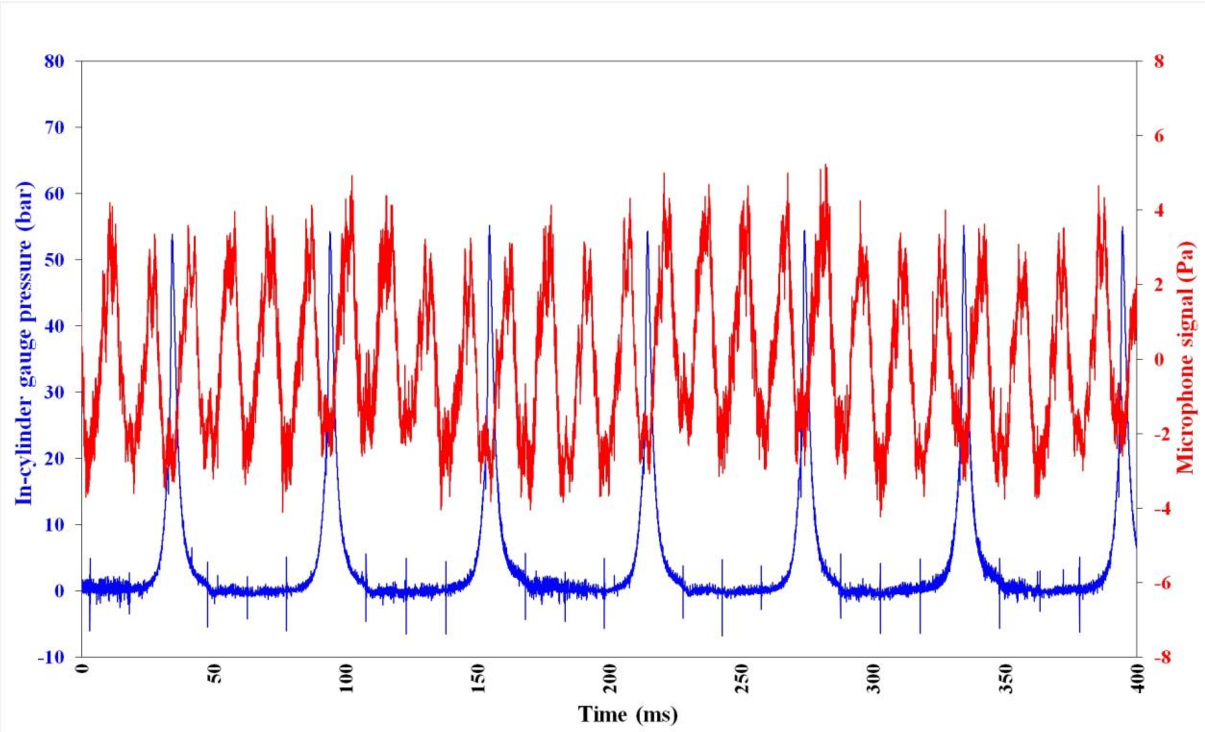

Fig. 8. Evolution with time of the in-cylinder (blue signal) and acoustic (red signal) pressures for a series of normal combustion cycles at engine speed of 2,000 rpm.

It can be seen that normal combustion cycles show in-cylinder peak pressures of about 55 bar and acoustic pressures oscillating within ± 3.5 Pa. In Fig. 9, three knocking combustion cycles can be clearly identified by peak in-cylinder pressures above 70 bar the (1st, 3rd and 7th cycles). In contrast, the acoustic pressure for these abnormal cycles show only slightly higher amplitudes (within ± 5 Pa) compared to those of the normal combustion cycles.

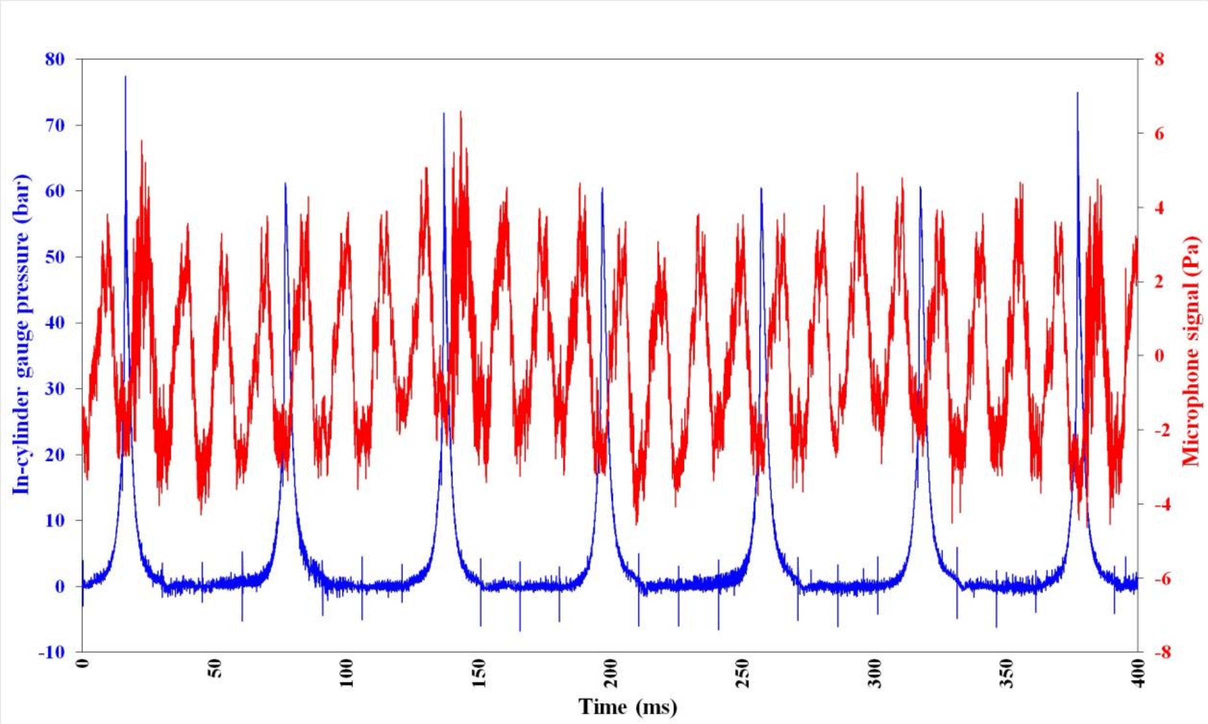

Fig. 9. Evolution with time of the in-cylinder (blue signal) and acoustic (red signal) pressures for a series of normal and abnormal combustion cycles at engine speed of 2,000 rpm.

A more in-depth characterization of the acoustic properties of a pair of normal and knocking combustion cycles is shown in Fig. 10 which presents a spectral analysis in terms of third octave bands. Octave-band analysis is incorporated by the most usual methods regarding the assessment of sound perception [41].

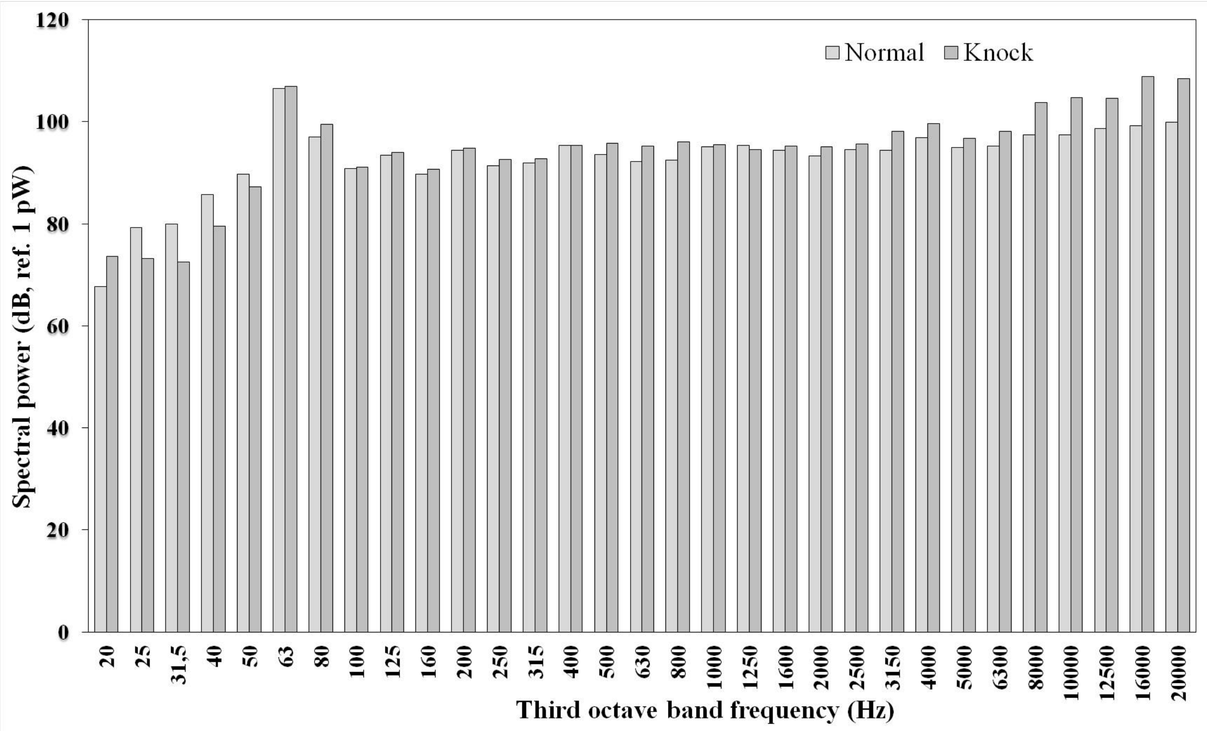

Fig. 10. Spectral analysis of typical normal and knocking cycles at engine speed of 2,000 rpm.

It can be seen that both cycles can be distinguished by means of the highest frequency bands (between 8 kHz and 20 kHz) which are around 8-10 dB more intense in the case of the knocking cycle than for the normal combustion. Furthermore, the spectral analysis is also useful to identify abnormal combustion phenomena associated to backfire. As mentioned in section 3.1. backfire was characterized by an abrupt increase of the intake air temperature accompanied by a strong hoarse noise. Fig. 11 shows the spectral power of a normal combustion cycle and two anomalous cycles consisting in knock and backfire, respectively. The number above the bars indicate the power change (in dB) with respect to the normal combustion cycle. It can be seen that backfire shows octave bands more intense by 7-16 dB in the range of frequencies comprised between 250 Hz and 4 kHz in comparison with the other combustion cycles.

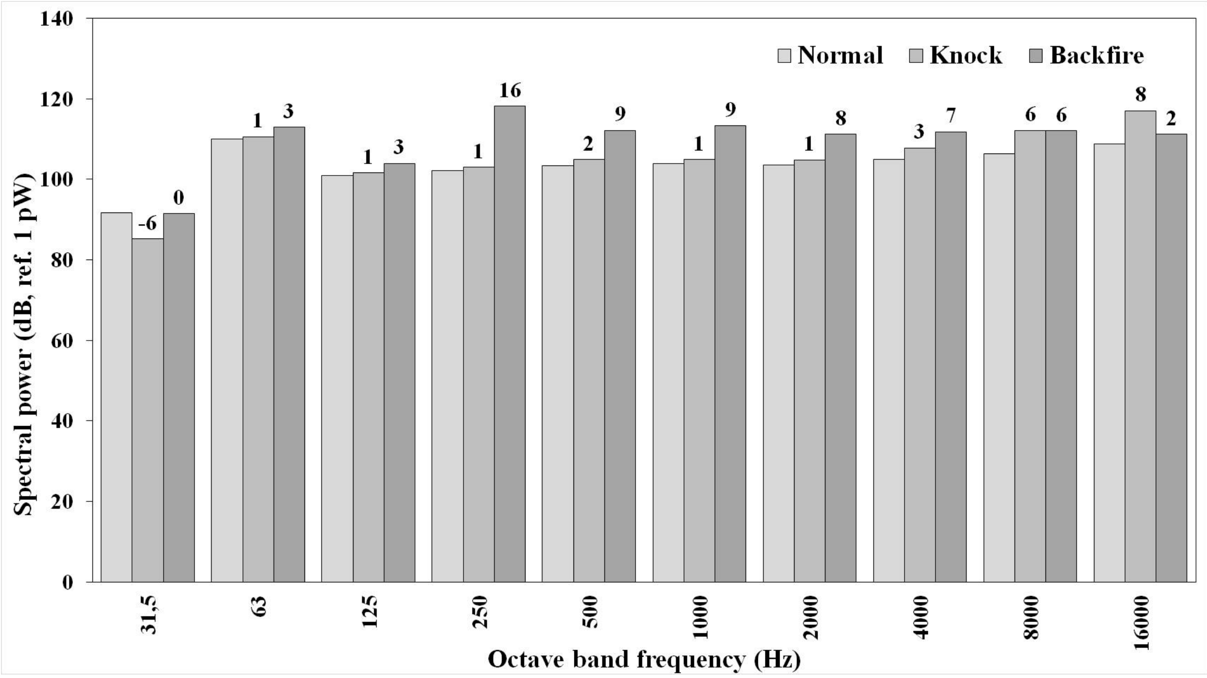

Fig. 11. Spectral analysis of typical normal, knocking and backfiring cycles at engine speed of 2,000 rpm.

4. Computational Fluid Dynamics (CFD) simulation of the engine performance

4.1. Aim and scope

In this work, a commercial Volkswagen 4-cylinder 1.4 L originally designed to be fed with gasoline and adapted to run on hydrogen has been used. One of the most important modifications performed consisted in the implementation of the hydrogen feeding system. In this regard, the original inlet manifold was replaced by another one made in metal for safer operation in the event of backfire. In addition, the gasoline injectors were replaced by gas injectors that were fixed to the inlet manifold by means of a metallic support and connected to a hydrogen accumulator through stainless steel tubing. The accumulator was necessary in order to guarantee that the injectors were supplied with hydrogen at a constant and suitably low pressure compared to the one in the gas cylinders that stored the fuel (200 bar).

Injection system configuration and its operating parameters such as injection timing and pulse width duration may have strong influence on the local fuel/air composition inside the intake manifold and cylinder. It was observed during the experiments that knock did not appear immediately after increasing the injection pulse width duration but it occurred some time after that, which suggested that hydrogen could be accumulating inside the manifold. To check this possibility, a computational fluid dynamics (CFD) study was conducted to simulate the performance of the hydrogen injection system used in this work. Simulations were accomplished using ANSYS-CFX® 15.0 software. The physical model consisted in the intake manifold, cylinder head and hydrogen injector geometries shown in Fig. 12.

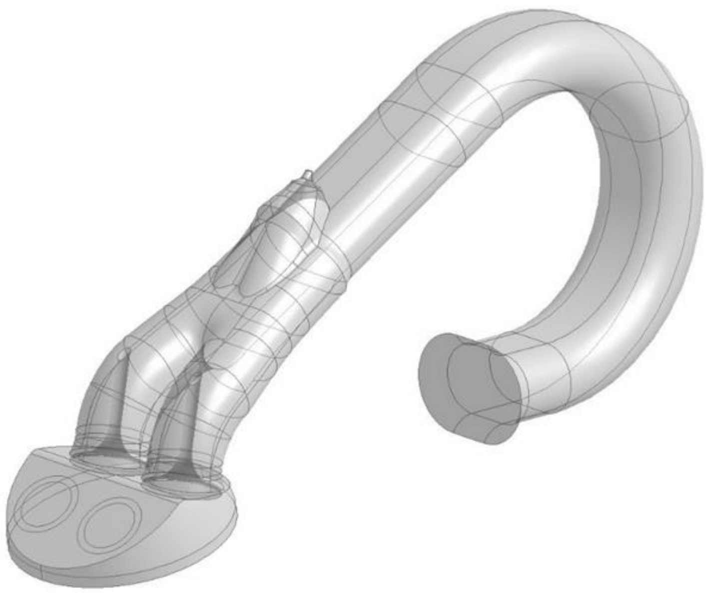

Fig. 12. Physical CFD model of the intake manifold, fuel injector and cylinder head.

4.2. Simulation conditions

Simulations were performed under transitory regime being TDC and the intake valve closing the initial and final instants, respectively. The following simplifying assumptions were adopted: hydrogen injection was considered isothermal at 25 ºC and buoyancy phenomena were neglected as transport was dominated by convective effects. On the other hand, the side of the intake manifold opposite to the cylinder was modeled as an open surface at constant manifold air pressure (MAP) allowing the entry of air due to the suction associated to the piston motion. MAP value was set at 0.92 bar according to the values recorded by the electronic control unit during the experiments performed at WOT. As concerns turbulence the k-ε model was adopted. After a preliminary study on grid independence of the solution, a moving grid with *ca.* 250,000 volume elements was adopted to describe the piston and valves motion.

The gas injectors used provided hydrogen at constant mass flow rate of 0.31 mg/ms during the pulse, being 1.2 ms and 0.2 ms the time required for the injector opening and closing, respectively. Injection timing was initially set at CA of 22 º ATDC. It should be noted that exhaust valve closing (EVC) timing was established at CA of 15.3 º in order to allow suitable cooling to reduce the likelihood of backfire.

As concerns the piston positioning, a value of 0 was assigned to TDC whereas the piston displacement adopted negative values given by the following expression obtained after considering the slider-crank engine geometry:

$$Z_p = -0.00402 + 0.0378 \cdot \cos\left[\left(\frac{2\pi}{60}\cdot n\right)\cdot t\right] + 0.0024 \cdot \cos\left[\left(\frac{4\pi}{60}\cdot n\right)\cdot t\right] \tag{1}$$

where Z_p (m) is the piston positioning, n (rpm) is the engine speed and t (s) is the time passed from the piston positioning at TDC. On the other hand, the positioning of the intake valve (Z_{iv}) was – 1.56 mm at TDC and was given (in m) by:

$$Z_{iv} = -0.0037 \cdot \left(\cos\left[\left(\frac{2\pi}{60}\cdot n\right)\cdot\frac{360}{214}\cdot t_0\right] - \cos\left[\left(\frac{4\pi}{60}\cdot n\right)\cdot\frac{360}{214}\cdot(t+t_0)\right]\right) \tag{2}$$

where t_0 (s) is the time passed between the start of the intake valve opening and the instant when the piston reaches TDC (*i.e.* the time required to turn the 19 º of crank angle corresponding to the intake valve opening advance).

4.3. Simulation results

Fig. 13 A-D includes a sequence of images showing the contour maps of hydrogen molar fraction in the intake manifold and cylinder during the intake stroke obtained from the CFD simulations of the engine running at 2,000 rpm. Hydrogen injection started at 22 º ATDC and the injection pulse width was 6 ms. Fig. 13 A shows that after 3.3 ms (40 º ATDC) when the injection is close to ending, the hydrogen concentrates near the injector. After 7.5 ms (Fig. 13 B, 90 º ATDC) the injection has finished and it can be seen that hydrogen has spread within the intake manifold whereas there is almost no hydrogen in the cylinder. Fig. 13 C shows that after 12.5 ms, at 150 º ATDC the great majority of hydrogen has entered the cylinder by the suction caused by the piston displacement. Finally, when the intake valve closes at 195 º ATDC (16.25 ms) some hydrogen still remains within the intake manifold as shown in Fig. 13 D. Depending on the evolution of the situation during the subsequent combustion cycles it is possible that an accumulation of hydrogen within the intake manifold takes place. In that case the mixture entering the cylinder will be richer than expected so the likelihood of knock will increase even maintaining constant the injector pulse width. As hydrogen is present within the intake manifold the risk of suffering from backfire during engine operation is evident; as a matter of fact, the backfire events detected in this work were preceded by knocking combustion cycles as explained in section 3.1. The results suggest that the temperature increase provoked by knock, together the presence of hydrogen in the intake manifold lead to combustion while the intake valve is open.

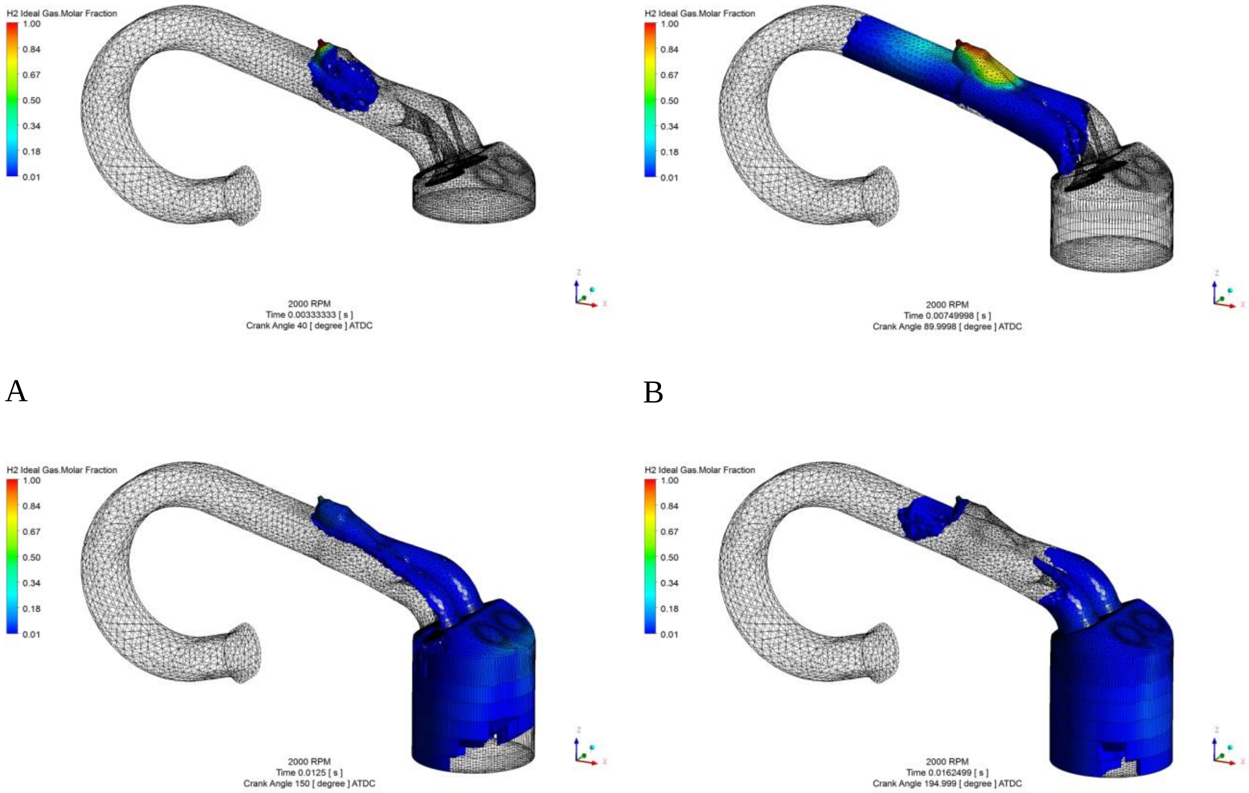

A B

C D

Fig. 13. Hydrogen molar fraction in the intake manifold and cylinder at CA values ATDC of: A) 40 º; B) 90 º; C) 150 º and D) 195 º (engine running at 2,000 rpm).

The problem of hydrogen accumulation could be due to the fact that the engine was designed to run on gasoline, that is, a liquid fuel with a density much higher than that of hydrogen. For that reason, the valves dimensions, which are suitable for gasoline PFI seem to be not so large as to guarantee a sufficiently high hydrogen volumetric flow rate. In this regard, Fig. 14 shows the evolution of the amounts of hydrogen and air that have entered the cylinder during the intake stroke according to the CFD simulations.

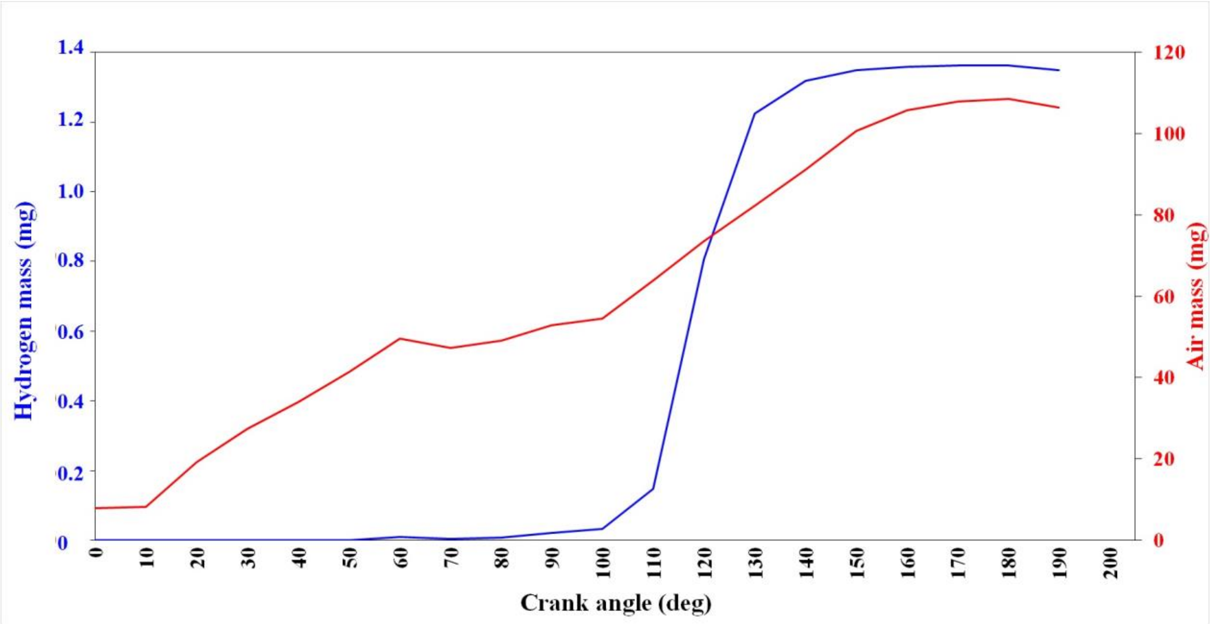

Fig. 14. CFD simulation results corresponding to the hydrogen (blue line) and air (red line) amounts in the cylinder during the intake stroke (engine running at 2,000 rpm).

It can be seen that the mass of air within the cylinder increases gradually until reaching bottom dead centre (BDC) at CA of 180 º. In contrast, the mass of hydrogen inside the cylinder increases sharply within a relatively narrow range of CA values between about 100 º and 140 º ATDC; afterwards, the amount of hydrogen remains almost constant. This is because the hydrogen injection is significantly retarded (22 º ATDC) in order to allow the cooling of the exhaust valve after closing. The very small decrease of the amount of gases observed ABDC may be due the pressure increase due to the beginning of the compression stroke and/or to a dragging effect associated to the intake valve closing.

The preceding results suggest that a possible solution would be advancing the injection time although the risk exists that the exhaust valve is still excessively hot. However, taking into account that the simulations were performed at an intermediate engine speed of 2,000 rpm and that running at higher speeds has to be feasible, advancing the injection time should be considered as a realistic option in order to attend the requirements of engine operation at highly demanding conditions. To investigate the effect of advancing the injection timing a series of CFD simulations were performed at injection times of 1 º and 22 º BTDC, injection pulse widths of 4 ms and 6 ms and engine speeds of 2,000 rpm and 4,000 rpm.

Table 1. Results of the CFD simulations performed at various H_2 injection conditions.

Engine speed (rpm)	Injection pulse width (ms)	Injection advance (º BTDC)	$\omega_{H_2}^{im}$ (%)
2,000	4	1	5
2,000	4	22	6
2,000	6	1	5
2,000	6	22	9
4,000	4	1	30
4,000	4	22	48
4,000	6	1	50
4,000	6	22	62

Table 1 shows the mass fraction of the hydrogen injected that remained in the intake manifold ($\omega_{H_2}^{im}$) after the intake valve closing. As expected, advancing the injection time has a positive effect on the introduction of hydrogen into the cylinder; however, the phenomenon is largely dominated by the engine speed. This is because the timing window available for injection decreases as the engine speed increases. So even greatly advancing the injection time (1 º BTDC) and reducing the injection pulse width (4 ms) the fraction of hydrogen that cannot enter the cylinder at 4,000 rpm is as high as 30 %. As a matter of fact, the majority of hydrogen (62 %) remained in the intake manifold at 4,000 rpm if the injection time is maintained at 22 º BTDC. Moreover, if the injection pulse width is relatively large, hydrogen would be injected at crank angles well above 160 º BTDC when the suction capacity of the cylinder is very limited. If this situation is maintained from cycle to cycle a non-steady situation is established leading to an accumulation of hydrogen that can provoke abnormal combustion events. Therefore, in addition to a suitable dimensioning of the valves, the design of the hydrogen injectors is another key factor. Indeed, as already mentioned, the injectors mounted deliver hydrogen at a mass flow rate of 0.31 mg/ms which seems to be insufficient for guaranteeing an operation free from backfire at high engine speeds.

Finally, suitable manifold design should take into account the speed of sound for proper tuning of the pressure waves and injector opening (intake manifold resonance charging). That speed is different for hydrogen-air mixtures than for the gasoline-air ones, which can also contribute to the accumulation of hydrogen.

5. Best engine performance

Taking into account the engine limitations some final experiments were carried out in order to determine its best possible output at conditions free from abnormal combustion events. To that end, after an initial warming-up period the hydrogen-air mixture fed to the four cylinders was progressively fuel-enriched by increasing the injection pulse width. The engine was operated at different speeds and the highest values of the brake torque and power that could be achieved in the absence of abnormal combustion events were determined in each case. The results are compiled in Table 2 where the values of injection pulse width and the air-to-fuel ratio have been also included.

It can be seen that the hydrogen-air mixture providing the best output becomes leaner (higher λ) as the engine speed increases. This could be due to the fact that at higher engine speeds the amount of hydrogen injected also increases as well as the fraction of the hydrogen that remained in the intake manifold, thus increasing the likelihood of provoking abnormal combustion events.

Whereas the highest value of the brake power (33.5 kW) was obtained at the maximum engine speed considered (5,000 rpm), the highest brake torque (67.2 N·m) resulted at 4,000 rpm. On comparing these values with the best engine performance achieved when gasoline is used as fuel (59 kW at 5,000 rpm and 132 N·m at 3,800 rpm) [6], it is clear that an output loss of about 50 % results when replacing gasoline by hydrogen. This is due to a great extent by the propensity of hydrogen to suffer from abnormal combustion phenomena which remarks the importance of their early and accurate detection.

Table 2. Best engine output at the speeds indicated and normal combustion conditions.

Engine speed (rpm)	Injection pulse width (ms)	Air-to-fuel ratio (λ)	Brake torque (N·m)	Brake power (kW)
1,000	7.59	1.30	50.3	5.27
2,000	7.85	1.35	63.5	13.3
3,000	7.92	1.42	65.4	20.5
4,000	8.42	1.49	67.2	28.1
5,000	8.76	1.52	64.0	33.5

6. Conclusions

A good correlation between in-cylinder pressure and block-engine acceleration measurements has been found regarding the detection of knocking combustion cycles in a port-fuel injection spark ignition internal combustion engine of automotive size fueled with hydrogen-air mixtures. To improve the accuracy, signals were decomposed into their low- and high-frequency components by means of conventional Fourier transform analysis. High and low frequencies were distinguished as the values above and below 20 times the engine speed, respectively. Knock events were very well described by the high-frequency components of the pressure and acceleration signals which showed changes associated to the abnormal combustion event of up to about 20 bar and 250 g, respectively. The adopted criterion, based on the engine speed, has the advantage of taking into account the important effects introduced by the engine speed in conditioning the likelihood of suffering abnormal combustion events.

To the best of our knowledge, in this work the in-cylinder pressure and block-engine vibration measurements are carried out simultaneously together with ambient noise recording for the first time. The raw signal recorded by the microphone allowed to detect the strong hoarse noise associated to backfire but it did not allow distinguishing knock from the background signal in spite of the characteristic pinging noise that could be heard during some combustion cycles. However, a spectral analysis of the raw signal in terms of third octave bands greatly improved the sensitivity. In this regard, a typical knocking cycle could be distinguished from a normal combustion cycle through the highest frequency bands (between 8 kHz and 20 kHz) which were *ca.* 8-10 dB more intense. As concerns backfire, this anomaly could be associated to more intense octave bands at the lowest frequencies (between 250 Hz and 4 kHz). These results indicate that detection of abnormal combustion events is possible through acoustic measurements. An optimization of the experimental conditions, particularly microphone location, will surely provide a much more accurate detection results that the ones achieved in this work. Therefore there is great potential for the development of acoustic sensors for abnormal combustion detection in automotive engines.

CFD simulations performed with a physical model that reproduced the engine systems for mixture formation and fuel injection revealed that combustion anomalies can arise as a result of the fact that the engine was originally designed to run on gasoline, a fuel much more dense than hydrogen. It has been found that a fraction of the hydrogen injected still remains in the intake manifold after the intake valve has closed. This fraction increases with the increase of the injection pulse width to obtain richer mixtures and especially when the engine speed rises (*e.g.* from 5-9 % at 2,000 rpm to 30-62 % at 4,000 rpm) due to the reduced time window available for fuel injection. The accumulation of hydrogen that takes place increases the risk of backfire which in turn increases the likelihood of suffering from knock events in the subsequent combustion cycles. The simulation results indicated that the dimension of the valves and the hydrogen flow rate delivered by the injectors were not sufficiently large as to assure that all the injected hydrogen enters the cylinders. The conclusion is that although the adaptation of gasoline engines to run on hydrogen is obviously feasible, a dedicated design is highly recommended when the engine will be fueled with hydrogen in order to avoid the problems associated to abnormal combustion phenomena.

Acknowledgements

We gratefully acknowledge Volkswagen Navarra S.A. for the Volkswagen Polo 1.4 engine donation. LMG and PMD thank the Spanish Ministerio de Economía, Industria y Competitividad (MINECO) and the European Regional Development Fund (ERDF/FEDER) for the financial support under project ENE2015-66975-C3-1-R.

References

[1] Gandía LM, Arzamendi G; Diéguez PM. Renewable Hydrogen Energy: An Overview. In: Gandía LM, Arzamendi G; Diéguez PM, editors. Renewable Hydrogen Technologies, Amsterdam: Elsevier; 2013, p. 1–17.

[2] Verhelst S. Recent progress in the use of hydrogen as a fuel for internal combustion engines. Int J Hydrogen Energy 2014; 39: 1071–85.

[3] Helmut E, Klaus S, Daniel L, Manfred K, Markus S. Potential of Synergies in a Vehicle for Variable Mixtures of CNG and Hydrogen. SAE Technical Paper 2009-01-1420; 2009: 19–28.

[4] Diéguez PM, Urroz JC, Marcelino-Sádaba S, Pérez-Ezcurdia A, Benito-Amurrio M, Sáinz D, et al. Experimental study of the performance and emission characteristics of an adapted commercial four-cylinder spark ignition engine running on hydrogen–methane mixtures. Appl Energy 2014; 113: 1068–76.

[5] Stockhausen WF, Natkin RJ, Kabat DM, Reams L, Tang X, Hashemi S, et al. Ford P2000 Hydrogen Engine Design and Vehicle Development Program. SAE Technical Paper 2002-01-0240; 2002: 63–71.

[6] Sopena C, Diéguez PM, Sáinz D, Urroz JC, Guelbenzu E, Gandía LM. Conversion of a commercial spark ignition engine to run on hydrogen: Performance comparison using hydrogen and gasoline. Int J Hydrogen Energy 2010; 35: 1420–9.

[7] Escalante Soberanis MA, Fernandez AM. A review on the technical adaptations for internal combustion engines to operate with gas/hydrogen mixtures. Int J Hydrogen Energy 2010; 35: 12134–40.

[8] Sáinz D, Diéguez PM, Sopena C, Urroz JC, Gandía LM. Conversion of a commercial gasoline vehicle to run bi-fuel (hydrogen-gasoline). Int J Hydrogen Energy 2012; 37: 1781–9.

[9] Verhelst S, Demuynck J, Sierens R, Scarcelli R, Matthias NS, Wallner T. Update on the Progress of Hydrogen-Fueled Internal Combustion Engines. In: Gandía LM, Arzamendi G; Diéguez PM, editors. Renewable Hydrogen Technologies, Amsterdam: Elsevier; 2013, p. 381–400.

[10] Heywood JB. Internal Combustion Engine Fundamentals. New York: McGraw-Hill Inc.; 1988.

[11] Verhelst S, Wallner T, Eichlseder H, Naganuma K, Gerbig F, Boyer B, et al. Electricity powering combustion: hydrogen engines. Proc IEEE 2012; 100: 427-39.

[12] White CM, Steeper RR, Lutz AE. The hydrogen-fueled internal combustion engine: a technical review. Int J Hydrogen Energy 2006; 31: 1292–305.

[13] Luo Q-h, Sun B-g. Experiments on the effect of engine speed, load, equivalence ratio, spark timing and coolant temperature on the energy balance of a turbocharged hydrogen engine. Energy Convers Manage 2018; 162: 1–12.

[14] Marseglia G, Costa M, Catapano F, Sementa P, Vaglieco BM. Study about the link between injection strategy and knock onset in an optically accessible multi-cylinder GDI engine. Energy Convers Manage 2017; 134: 1–19.

[15] Verhelst S, Wallner T. Hydrogen-fueled internal combustion engines. Prog. Energy Combust. Sci. 2009; 35: 490–527.

[16] Zhen X, Wang Y, Xu S, Zhu Y, Tao C, Song M. The engine knock analysis – An overview. Appl Energy 2012; 92: 628–36.

[17] Wang Z, Liu H, Reitz RD. Knocking combustion in spark-ignition engines. Prog. Energy Combust. Sci. 2017; 61: 78–112.

[18] Pan J, Sheppard CGW. A Theoretical and Experimental Study of the Modes of End Gas Autoignition Leading to Knock in S.I. Engines. SAE Technical Paper 942060; 1994: 1925–47.

[19] Fiołka J. Fractional Fourier Transform and its Application to Engine Knock Detection. Proceedings of the 22nd International Conference "Mixed Design of Integrated Circuits and Systems", June 25-27, 2015, Toruń, Poland, p. 595–8.

[20] Pan J, Shu G, Wei H. Research on in-cylinder pressure oscillation characteristic during knocking combustion in spark-ignition engine. Fuel 2014; 120: 150–7.

[21] Su T, Ji C, Wang S, Shi L, Yang J, Cong X. Effect of spark timing on performance of a hydrogen-gasoline rotary engine. Energy Convers Manage 2017; 148: 120–7.

[22] Božić M, Vučetić A, Sjerić M, Kozarac D, Lulić Z. Experimental study on knock sources in spark ignition engine with exhaust gas recirculation. Energy Convers Manage 2018; 165: 35–44.

[23] Li H, Karim GA. Knock in spark ignition hydrogen engines. Int J Hydrogen Energy 2004; 29: 859–65.

[24] Bradley D, Kalghati GT. Influence of autoignition delay time characteristics of different fuels on pressure waves and knock in reciprocating engines. Combust Flame 2009; 156: 2307-2318.

[25] Rosseel E, Sierens R. Knock Detection in a Hydrogen Engine. SAE Technical Paper 970039; 1997: 37–47.

[26] Tang X, Kabat DM, Natkin RJ, Stockhausen WF, Heffel J. P2000 Hydrogen Engine Dynamometer Development. SAE Technical Paper 2002-01-0242; 2002: 81–92.

[27] Szwaja S, Bhandary KR, Naber JD. Comparison of hydrogen and gasoline combustion knock in a spark ignition engine. Int J Hydrogen Energy 2007; 32: 5076–87.

[28] Kawahara N, Tomita E. Visualization of auto-ignition and pressure wave during knocking in a hydrogen spark-ignition engine. Int J Hydrogen Energy 2009; 34: 3156–63.

[29] Szwaja S, Naber JD. Dual nature of hydrogen combustion knock. Int J Hydrogen Energy 2013; 38: 12489–96.

[30] Yang F, Zhang H, Chen Z, Kong W. Interaction of pressure wave and propagating flame during knock. Int J Hydrogen Energy 2013; 38: 15510–9.

[31] Sun B, Tian H, Liu F. The distinctive characteristics of combustion duration in hydrogen internal combustion engine. Int J Hydrogen Energy 2014; 39: 14472–8.

[32] Luo Q, Sun B. Inducing factors and frequency of combustion knock in hydrogen internal combustion engines. Int J Hydrogen Energy 2016; 41: 16296–305.

[33] Kiesgen G, Klüting M, Bock C, Fischer H. The New 12-Cylinder Hydrogen Engine in the 7 Series: The H_2 ICE Age Has Begun. SAE Technical Paper 2006-01-0431; 2006: 13–21.

[34] Scholl D, Barash T, Russ S, Stockhausen W. Spectrogram Analysis of Accelerometer-Based Spark Knock Detection Waveforms. SAE Technical Paper 972020; 1997: 1183–90.

[35] Boubai O. Knock Detection in Automobile Engines. IEEE Instrum Meas Mag September; 2000: 25–8.

[36] Naber JD, Blough JR, Frankowski D, Goble M, Szpytman JE. Analysis of Combustion Knock Metrics in Spark-Ignition Engines. SAE Technical Paper 2006-01-0400; 2006: 111–32.

[37] Brunt MFJ, Pond CR, Biundo J. Gasoline Engine Knock Analysis using Cylinder Pressure Data. SAE Technical Paper 980896; 1998: 1399–412.

[38] Li T, Yin T, Wang B. A phenomenological model of knock intensity in spark-ignition engines. Energy Convers Manage 2017; 148: 1233–47.

[39] Shen X, Zhang Y, Shen T, Khajornstraidet C. Spark-advance self-optimization with knock probability threshold for lean-burn operation mode of SI engine. Energy 2017; 122: 1–10.

[40] Redel-Macías MD, Hervás-Martínez C, Gutiérrez PA, Pinzi S, Cubero-Atienza AJ, Dorado MP. Computational models to predict noise emissions of a diesel engine fueled with saturated and monounsaturated fatty acid methyl esters. Energy 2018; 144: 110–9.

[41] Redel-Macías MD, Pinzi S, Leiva D, Cubero-Atienza AJ, Dorado MP. Air and noise pollution of a diesel engine fueled with olive pomace oil methyl ester and petrodiesel blends. Fuel 2012; 95: 615–21.